Supporting Information

Constructing and controlling of ruthenium active phases for acetylene hydrochlorination

Bolin Wang,[a, b, ‡] Yuxue Yue,[a, ‡] Saisai Wang,[a] Zhi Chen,[a] Lu Yu,[a] Shujuan Shao,[a] Guojun Lan,[a] Zhiyan Pan,[b] Jia Zhao[a,*] and Xiaonian Li[a,*]

[a] Industrial Catalysis Institute of Zhejiang University of Technology, Hangzhou, 310014, People's Republic of China

[b] College of Environment of Zhejiang University of Technology, Hangzhou, 310014, People's Republic of China

[‡] These authors contributed equally.

* Corresponding author. Tel: +86 571 88871656. E-mail address: jiazhao@zjut.edu.cn (Jia Zhao)

* Corresponding author. Tel: +86 571 88320002. E-mail: xnli@zjut.edu.cn (Xiaonian Li)

1. Experimental

1.1 Catalyst Preparation

Ru^0/C: In a typical experiment, a solution of $RuCl_3$ (0.5 mmol) precursor was dissolved in 1-butyl-3-methylimidazolium bis ((trifluoromethyl) sulfonyl) imide BMIM-NTf_2 (10 mL) via syringe under an argon (Ar) flow, resulting in a turbid dispersion. Then activated carbon (C, NORIT, ROX 0.8) carrier was added to the above solution under 50 ºC and hydrogen (4 bar) conditions for 18 h. Subsequently, the prepared sample was thermally activated at 500 ºC for 2h.

RuO_2/C: In a Fischer-Porter bottle, a solution of $RuCl_3$ (0.5 mmol) was dissolved in 10 mL of 1-butyl-3-methylimidazolium hexafluorophosphate BMIM-PF_6 by heating (50 ºC) and stirring under argon. The resulting solution was cooled to room temperature and added an excess of solid $NaBH_4$. Then activated carbon (C) carrier was added to the above solution under 50 ºC for 2 h under reduced pressure. Subsequently, the prepared sample was thermally activated at 500 ºC for 2h under Ar.

Ru SAC：A solution of $RuCl_3$ (0.5 mmol) was dissolved in 10 mL of 1-butyl-3-methylimidazolium chloride BMIM-Cl by heating (50 ºC) and stirring under argon. Then, activated carbon (C) carrier was added to the above solution with agitated stirring. Subsequently, the prepared sample was thermally activated at 400 ºC for 2h under Ar.

For Ru-N SAC catalysts, all synthesis steps were similar to Ru SAC except that BMIM-Cl is replaced by 1-butyl-3-methylimidazolium dicyanamide BMIM-$N(CN)_2$. Unless specifically mentioned, the mass loading of all Ru-based catalysts (Ru^0/C, RuO_2/C, Ru SAC, Ru-N SAC) was maintained at 0.5 wt.%.

Figure S1 shows the structure of the selected ionic liquids (ILs): (a) 1-butyl-3-methylimidazolium bis ((trifluoromethyl) sulfonyl) imide BMIM-NTf_2; (b) 1-butyl-3-methylimidazolium hexafluorophosphate BMIM-PF_6 and (c) 1-butyl-3-methylimidazolium chloride BMIM-Cl.

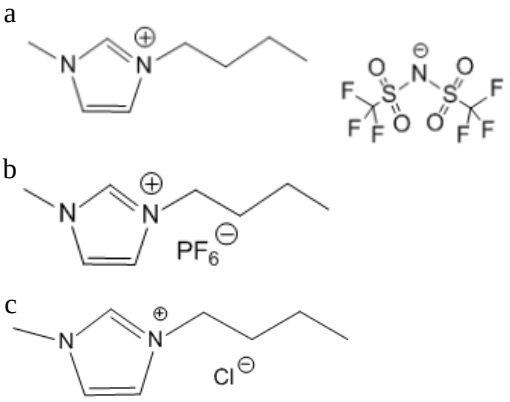

Figure S1 The structure of the selected ionic liquids (ILs): (a) 1-butyl-3-methylimidazolium bis ((trifluoromethyl) sulfonyl) imide BMIM-NTf_2; (b) 1-butyl-3-methylimidazolium hexafluorophosphate BMIM-PF_6 and (c) 1-butyl-3-methylimidazolium chloride BMIM-Cl.

1.2 Catalyst Characterization and Computational Details

The atomic-resolution images were obtained by a JEOL JEM-ARM 200F aberration-corrected scanning transmission electron microscopy (AC-STEM) operating at 200 kV in high-angle annular dark-field (HAADF) mode. The carbon powder was dispersed dry onto holey-carbon coated copper grids. Scanning electron microscopy (SEM) morphology was evaluated with a Philips XL-30 scanning electron microscope. Nitrogen adsorption/desorption isotherms (BET) is acquired from a Micromeritics ASAP 2020. The X-ray absorption (EXAFS) experiments were carried out at the XAS station (BL14W1) of the Shanghai Synchrotron Radiation Facility (SSRF). The electron storage ring was operated at 3.5 GeV. Si (311) double-crystal was used as the

monochromator, and the data was collected using solid-state detector under ambient conditions. The beam size was limited by the horizontal and vertical slits with a surface area of 1×4 mm^2 during XAS measurements. The X-ray absorption of Ru foil at Ru K-edge was measured for energy calibration. The obtained XAFS data was processed in Athena (version 0.9.25) for background, pre-edge line and post-edge line calibrations. Then Fourier transformed fitting was carried out in Artemis (version 0.9.25). The k_2 weighting, k-range of ~3-12 Å and R range of 1-3 Å were used. The four parameters, coordination number, bond length, Debye-Waller factor and E^0 shift (CN, R, σ^2, ΔE^0) were fitted without anyone was being fixed, constrained, or correlated. X-ray photoelectron spectroscopy (XPS) was conducted by a Kratos AXIS Ultra DLD spectrometer. The solids were analyzed at the electron take-off angle of 45° and the pass energy of 46.95 eV. Temperature-programmed desorption (TPD) measurements is conducted with an Omnistar GSD320 mass spectrometer. All density functional theory (DFT) calculations were carried out using the Cambridge Sequential Total Energy Package known as CASTEP. Information regarding to the electron-electron interaction can be obtained from the exchange–correlation function under the generalized gradient approximation (GGA) with norm-conserving pseudopotentials and Perdew-Burke-Ernzerhof functional. The geometry optimization and electronic structure calculation were carried out using the Monkhorst-Pack special k-point meshes of 10 × 10 × 10 with a kinetic energy cut-off at 750 eV. During the geometry optimization, all atoms were allowed to relax without any constraints until the convergence thresholds of maximum displacement were reached, maximum force and energy were smaller than 0.001 Å,

0.03 eV/Å and 1.0×10^{-5} eV/atom, respectively.

1.3 Catalyst Testing

Catalytic performance of acetylene hydrochlorination was carried out in a fixed bed glass reactor (i.d. 10 mm, **Figure S2**). Firstly, the reactor containing catalyst was flushed using nitrogen gas (N_2) for 0.5 h at 160 °C. Then, reaction gas mixture of C_2H_2 and HCl was fed into the cleaned reactor at a gas hourly space velocity of C_2H_2 (GHSV) of 1000 h^{-1}, C_2H_2 : HCl ratio was kept constant at a value of 1 : 1.2. The exitting gas from the reactor was passed through a saturated NaOH solution in an absorption bottle to remove any unreacted HCl before it was sent to be analyzed by an online gas chromatography (GC 9790, Zhejiang Fuli Analytical Instruments Co., Ltd.). The catalytic activity is presented as the conversion of acetylene, $X_{(C2H2)}$, calculated according to Eq. 1,

$$X_{C2H2}=\frac{n(C_2H_2)^{intlet}-n(C_2H_2)^{outlet}}{n(C_2H_2)^{intlet}}\times 100\% \qquad \text{Eq.1}$$

Where $n(C_2H_2)^{intlet}$ and $n(C_2H_2)^{outtlet}$ denote the respective molar flows of C_2H_2 at the reactor outlet and inlet.

The turnover frequency (TOF) is calculated according to Eq.2 ,

$$TOF = \frac{n(C_2H_2)^{intlet}-n(C_2H_2)^{outlet}}{mol_{Ru}\cdot h} \qquad \text{Eq.2}$$

The error of the carbon balance is presented as ε_C, calculated according to Eq. 3.[9] Where $n(VCM)^{outlet}$ denote the respective molar flows of VCM at the reactor outlet.

$$\varepsilon_C=\frac{n(C_2H_2)^{intlet}-n(C_2H_2)^{outlet}+n(VCM)^{outlet}}{n(C_2H_2)^{intlet}} \qquad \text{Eq.3}$$

The carbon balance is ≥ 98% in all experiments.

All catalytic data points were determined as an average of at least two measurements. According to Weisz-Prater Criterion and Mears Criterion [10] (Section 2 of *Supporting Information*), the internal and external mass transfer limitations are insignificant in the evaluation system of this work.

2. Absence of mass transport and heat transfer during kinetic measurements

2.1 Internal and external diffusion

The absence of mass transport resistances was checked by Weisz-Prater criterion (C_{WP}) for internal diffusion and Mears' criterion (C_M) for external diffusion.

$$C_{WP} = \frac{r_{obs}\rho_b R_p^2}{D_{eff}C_s} < 1 \qquad \text{Eq.4}$$

$$C_M = \frac{r_{obs}\rho_b R_P n}{k_c C_s} < 0.15 \qquad \text{Eq.5}$$

Where $r_{obs=}\frac{n(C_2H_2)^{inlet}-n(C_2H_2)^{outlet}}{m_{Cat}\cdot S}$, observed reaction rate: 0.082 mol/kg_{cat}·s

n= reaction order, estimated at a maximum value of 2

R_p= catalyst particle radius: $6.25\cdot10^{-5}$ m

ρ_b = bulk density of catalyst bed: 430 kg·m^{-3}

D_{eff} = effective diffusivity, estimated at a value of 8.9×10^{-6} m^2/s

C_s = gas concentration at the external surface of the catalyst: 14 mol·m^{-3}

k_c = external mass transfer coefficient, estimated at a value of 0.142 m/s

$$C_{WP} = \frac{r_{obs}\rho_b R_p^2}{D_{eff}C_s} \qquad \text{Eq.6}$$

$= [(0.082\ \text{mol/kg}_{cat}\cdot\text{s}) \times (430\ \text{kg/m}^3) \times (6.25\times10^{-5}\ \text{m})^2] / [(8.9\times10^{-6}\ \text{m}^2/\text{s}) \times (14\ \text{mol}/\text{m}^3)]$

$= 1.7\times10^3 << 1$

$$C_M = \frac{r_{obs}\rho_b R_P n}{k_c C_s} \qquad \text{Eq.7}$$

= [(0.082 mol/kg_{cat}·s) × (430 kg/m^3) × (6.25×10^{-5} m) × (2)] / [(0.142 m/s) × (14 mol /m^3)] = 2.2×10^{-3} < < 0.15

Therefore, internal and external diffusion effects could be neglected during the kinetic experiments.

2.2 Heat transfer

The absence of heat transfer was checked by Mears' criterion.

$$C_M = \left|\frac{-\Delta H r_{obs} \rho_b R_p E}{h T^2 R_g}\right| \quad \text{Eq.8}$$

Where ΔH= heat of reaction: -98.9 kJ/mol

r_{obs}=0.082 mol/kg_{cat}·s

ρ_b = bulk density of catalyst bed: 430 kg·m^{-3}

R_b = catalyst particle radius: $6.25\cdot10^{-5}$ m

E= activation energy, estimated at a value of 42 kJ/mol

h=heat transfer coefficient between gas and pellet, estimated at a value of 8.3×10^{-2} kJ/m^2·s·K

R_g= gas constant: 8.314×10^{-3} kJ/mol·K

T = reaction temperature, 433.15 K

$$C_M = \left|\frac{-\Delta H r_{obs} \rho_b R_p E}{h T^2 R_g}\right| \quad \text{Eq.9}$$

= [(98.9 kJ/mol)×(0.082 mol/kg_{cat}·s)×(430 kg/m^3)×(6.25×10^{-5} m)×42 kJ/mol] / [(8.3×10^{-2} kJ/m^2·s·K)×(433.15 K)^2×8.314×10^{-3} kJ/mol·K] = 0.069 << 0.15

Therefore, heat transfer effect during the kinetic experiment could be neglected.

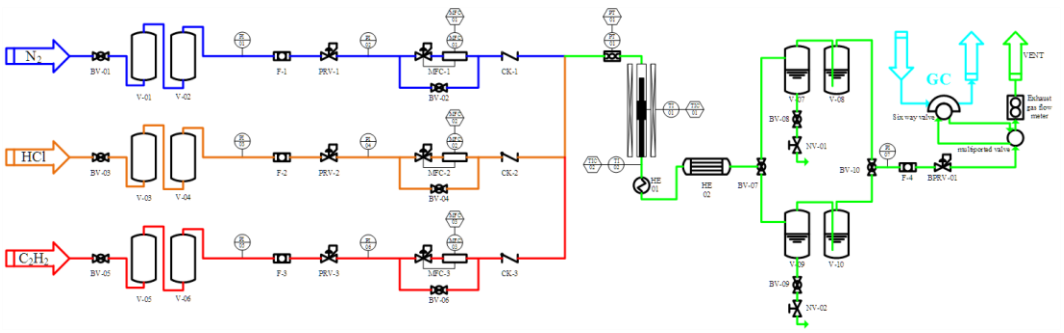

Figure S2. Schematic representation of the experimental rig as applied in the here reported continuous flow, gas phase acetylene hydrochlorination experiments [1].

Table S1 Fitting parameters from the EXAFS spectra of selected Ru-based catalysts.

Sample	Scattering path	CN[a]	R (Å)[b]	$\sigma^2\times10^3$ (Å^2)[c]	ΔE (eV)[d]	R factor
Ru foil	Ru-Ru	12	2.67±0.004	3.3±0.5	-4.3±0.8	0.008
$RuCl_3$	Ru-Cl	2.9±0.4	2.33±0.01	5.2±2.5	-1.9±0.7	0.007
Ru SAC	Ru-Cl	2.7±0.5	2.33±0.01	5.1±2.2	-1.2±2.0	0.010
Ru-N SAC	Ru-Cl Ru-N	2.2±0.4 1.1±0.4	2.33±0.01 2.02±0.03	5.1±2.0	-0.6±1.7	0.009

[a]Coordination number. [b]Coordination shell distance. [c]Debye-Waller factor. [d]Energy shift.

Table S2 TOF of different Ru-based catalysts.

Catalyst	Temperature °C	GHSV h^{-1}	TOF h^{-1}	Reference
Ru/SAC	170	1080	319	2
Ru/SAC-C200	170	1080	434	2
Ru/SAC-C300	170	1080	778	2
Ru/SAC-C400	170	1080	310	2
Ru/SAC-R300	170	1080	347	2
Ru/SAC-R400	170	1080	409	2
Ru/SAC-R500	170	1080	367	2
Ru-10%DMPU/AC	170	900	1590	3
Ru/AC	170	900	114	3
Ru1Co3/AC	170	900	29	3
Ru/3AC-N700	170	900	360	3
Ru/in-CNT	170	900	240	3
Ru/AC-NHN	170	900	110	3
Ru/AC-C300	170	900	612	3
Ru1K1/AC	170	900	65	3
Ru1Co3Cu1/AC	170	900	55	4
Hg/AC	170	900	12	5
Ru-N SAC[a]	160	6000	5263	This work
Ru SAC[a]	160	6000	2969	This work
RuO_2/C[a]	160	6000	329	This work
Ru^0/C[a]	160	6000	9	This work

[a] The catalysts developed in this work. Reaction conditions: 160 °C, C_2H_2 GHSV = 18000 h^{-1}, $V(HCl)/V(C_2H_2) = 1.2$.

Table S3. Reaction schemes of acetylene hydrochlorination on RuO_2/C and Ru SAC. Corresponding to the energy profiles shown in Figure 3a and Figure 3b.

RuO_2/C	
Step	Description
Ads.	* + HCl ↔ *HCl
TS	*HCl + C_2H_2 ↔ HCl*C_2H_2
Rea.	HCl*C_2H_2 ↔ C_2H_3Cl*
Dea.	C_2H_3Cl* ↔ C_2H_3Cl + *

* adsorption sites.

Table S4. Reaction schemes of acetylene hydrochlorination on Ru SAC. Corresponding to the energy profiles shown in Figure 3b.

Ru SAC	
Step	Description
Ads.	* + C_2H_2 ↔ *C_2H_2
TS	*C_2H_2 + HCl ↔ HCl*C_2H_2
Rea.	HCl*C_2H_2 ↔ C_2H_3Cl*
Dea.	C_2H_3Cl* ↔ C_2H_3Cl + *

* adsorption sites for Ru SAC.

Table S5. Reaction schemes of acetylene hydrochlorination on Ru-N SAC. Corresponding to the energy profiles shown in Figure 3c.

Ru-N SAC	
Step	Description
Ads.	* + C_2H_2 ↔ *C_2H_2
	* + HCl↔ *HCl
TS	*C_2H_2 + *HCl ↔ *HCl*C_2H_2
Rea.	*HCl*C_2H_2 ↔ C_2H_3Cl* + *
Dea.	C_2H_3Cl* ↔ C_2H_3Cl + *

* adsorption sites for Ru-N SAC.

Table S6. Element contents determined by XPS analysis over selected Ru-N SAC.

Sample	C wt.%	N(O) wt.%	Cl wt.%	Ru wt.%	Cl/C
RuO_2/C Fresh	98.1	1.1(O)	0.1	0.7	0.001
RuO_2/C Used	94.9	0.9(O)	3.5	0.7	0.04
Ru-N SAC 400 ℃ Fresh	95.3	3.2	0.9	0.6	0.009
Ru-N SAC 400 ℃ Used	95.2	2.9	1.2	0.7	0.01

Table S7. Impurities in industrial grade and laboratory level of reaction gases.

Impurity	Industrial grade (ppm)	Laboratory level (ppm)
Moisture	10	1.5
O_2	125	1
N_2	500	2
CO_2	15	5
H_2	350	/
H_2S	250	/

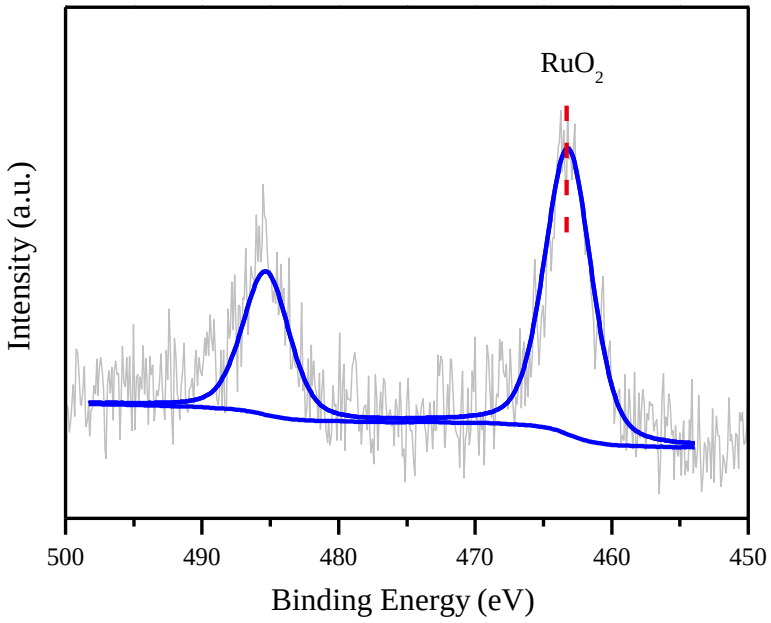

Figure S3 Ru 3p3 XPS spectra of RuO_2.

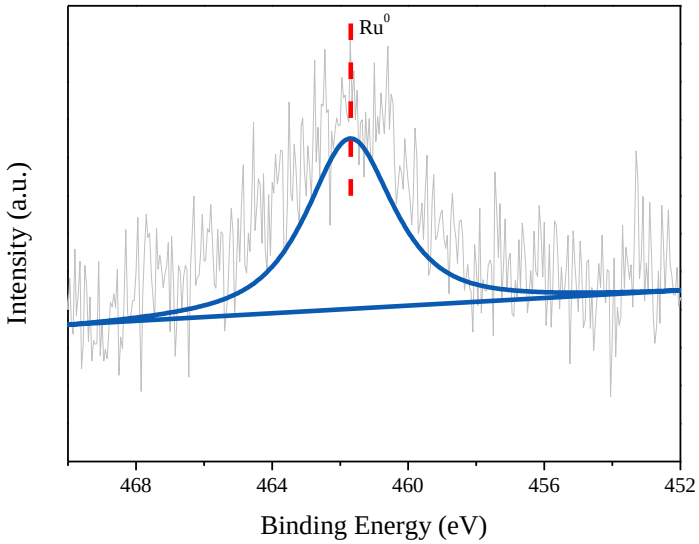

Figure S4 Ru 3p3 XPS spectra of Ru^0.

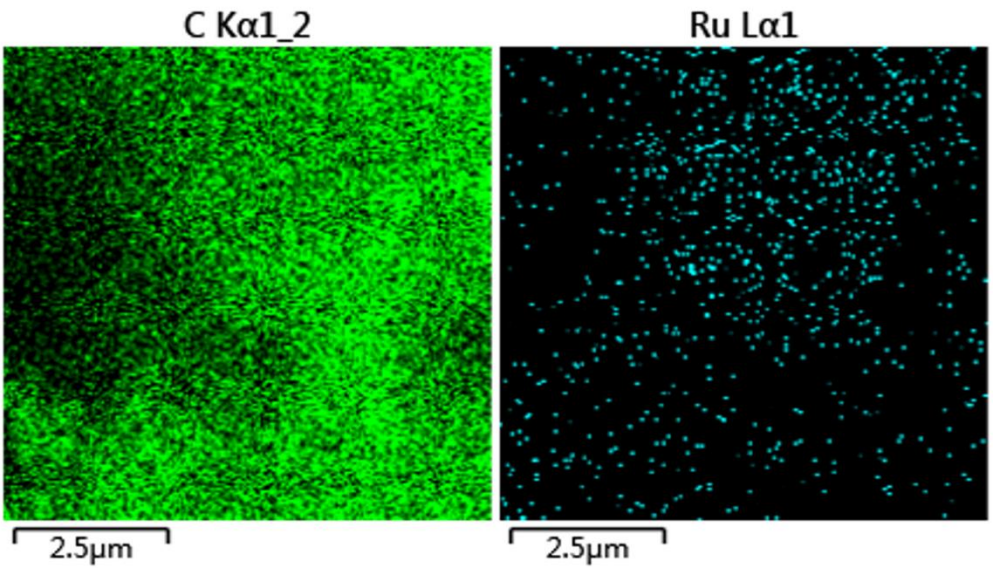

Figure S5 SEM image and elemental mapping of Ru^0/C.

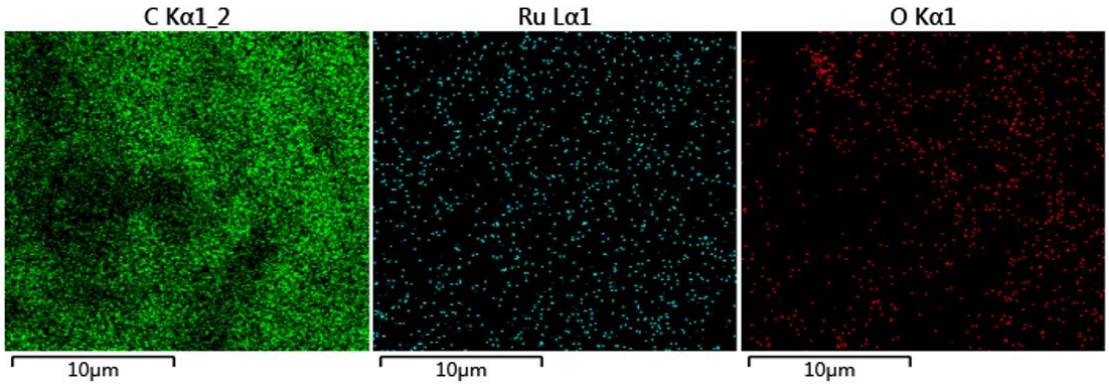

Figure S6 SEM image and elemental mapping of RuO_2/C.

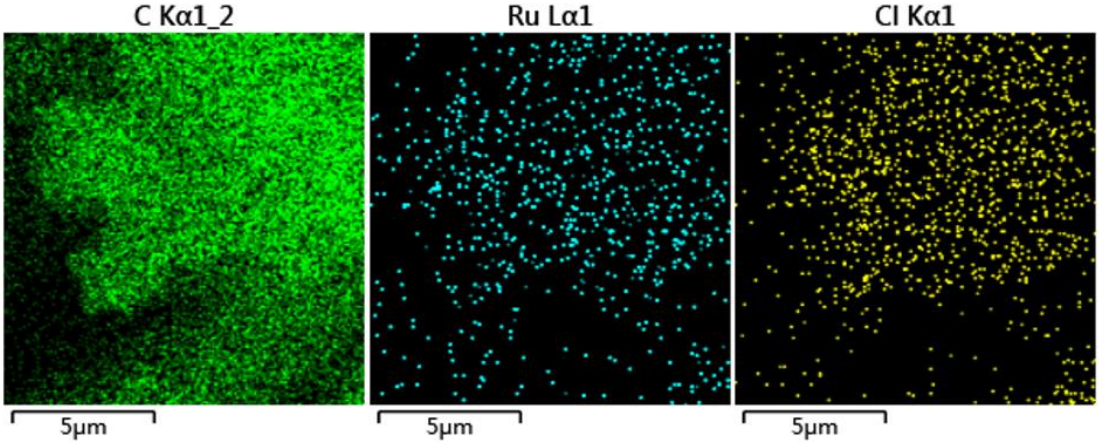

Figure S7 SEM image and elemental mapping of Ru SAC.

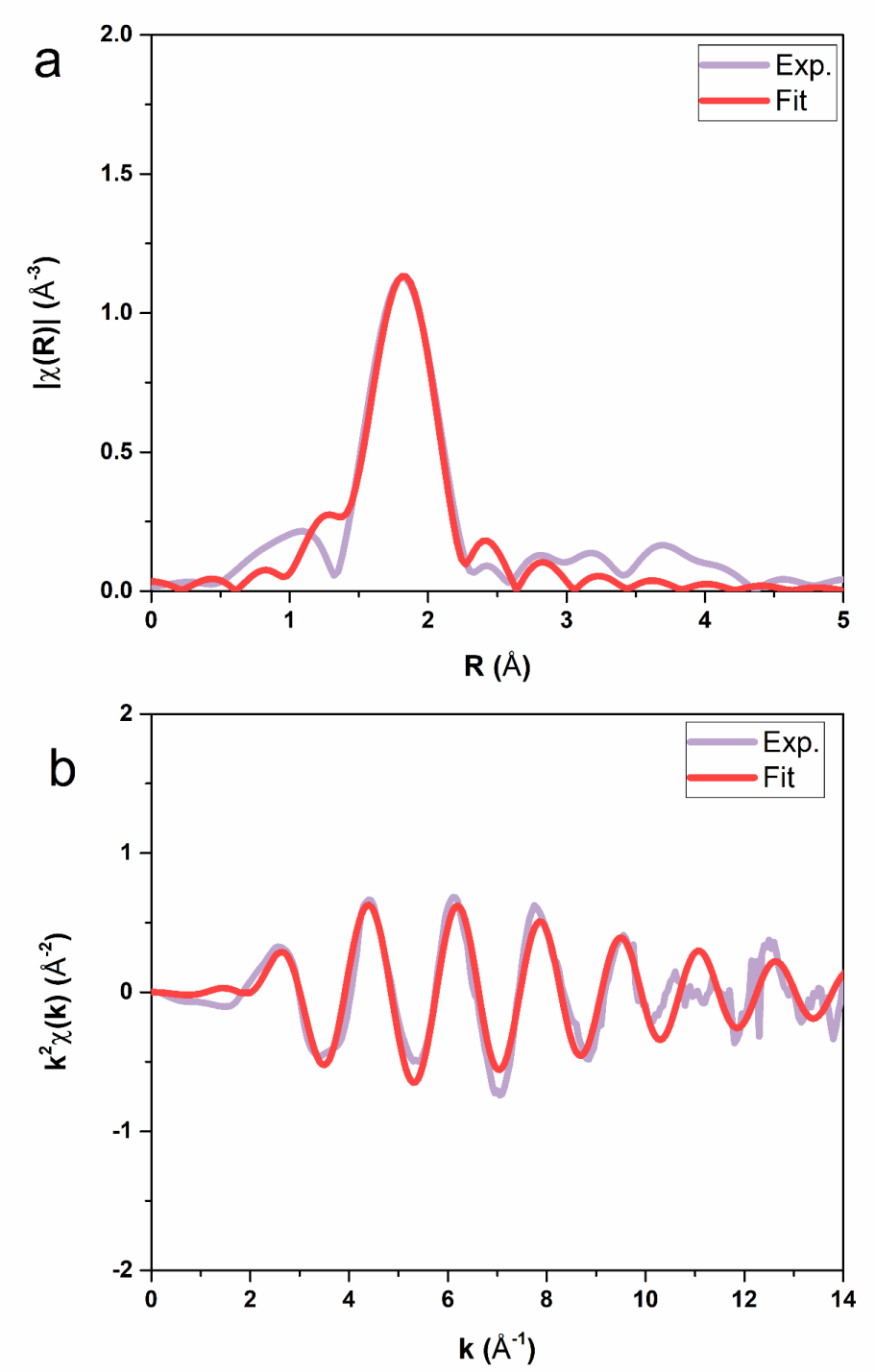

Figure S8 Ex situ Ru K edge-normalized XANES spectra of Ru SAC.

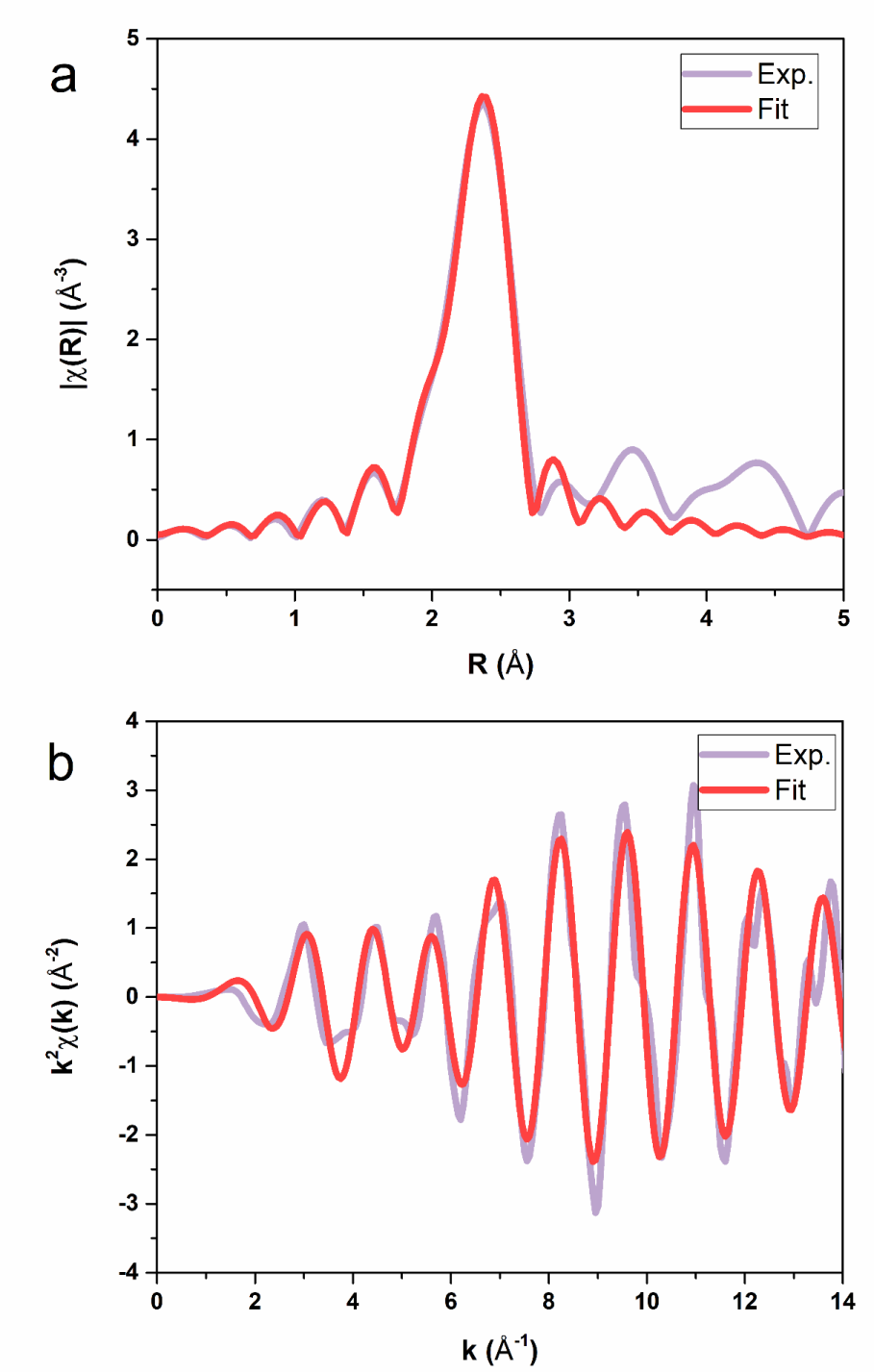

Figure S9 Ex situ Ru K edge-normalized XANES spectra of Ru foil.

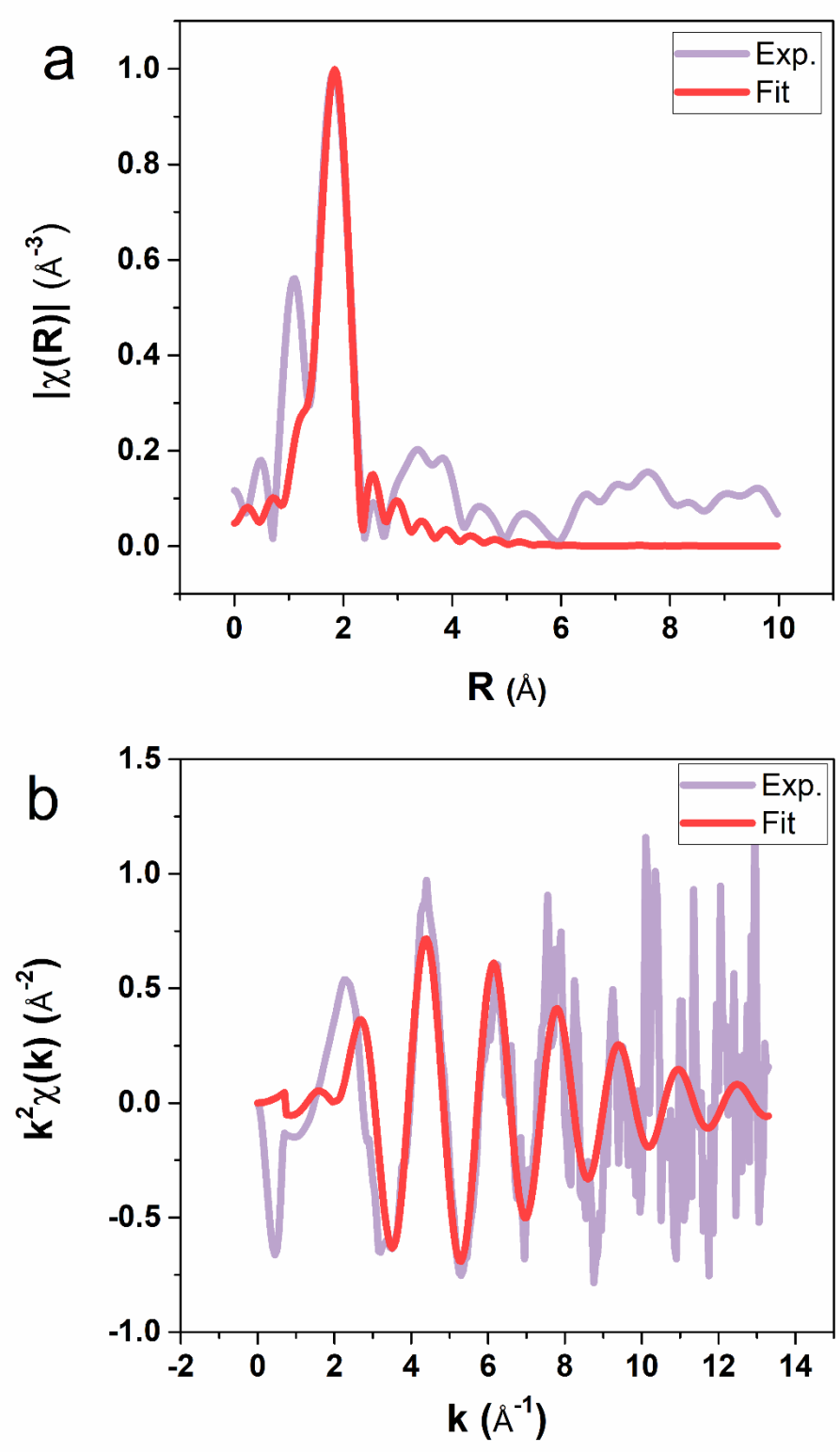

Figure S10 FT-EXAFS spectra of $RuCl_3$.

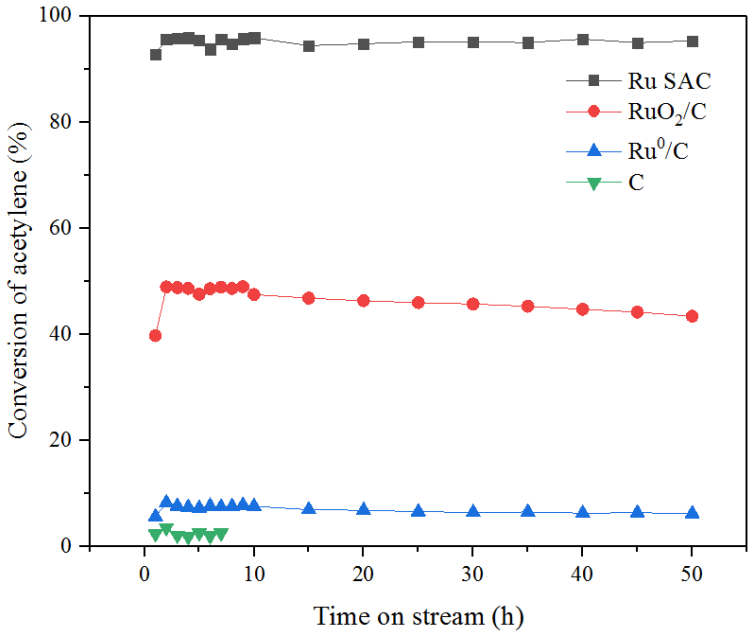

Figure S11 C_2H_2 Conversion of different Ru-based catalysts. Reaction conditions: 160 ºC, C_2H_2 GHSV = 1000 h^{-1}, V(HCl)/V(C_2H_2) = 1.2.

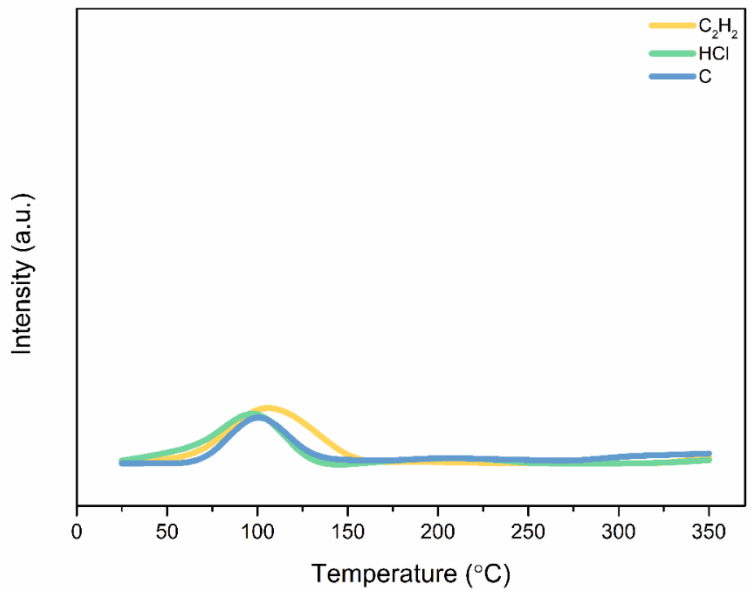

Figure S12 C_2H_2 and HCl TPD of Ru^0/C under individual gas (C_2H_2 or HCl). For C carrier, only acetylene signal is detected.

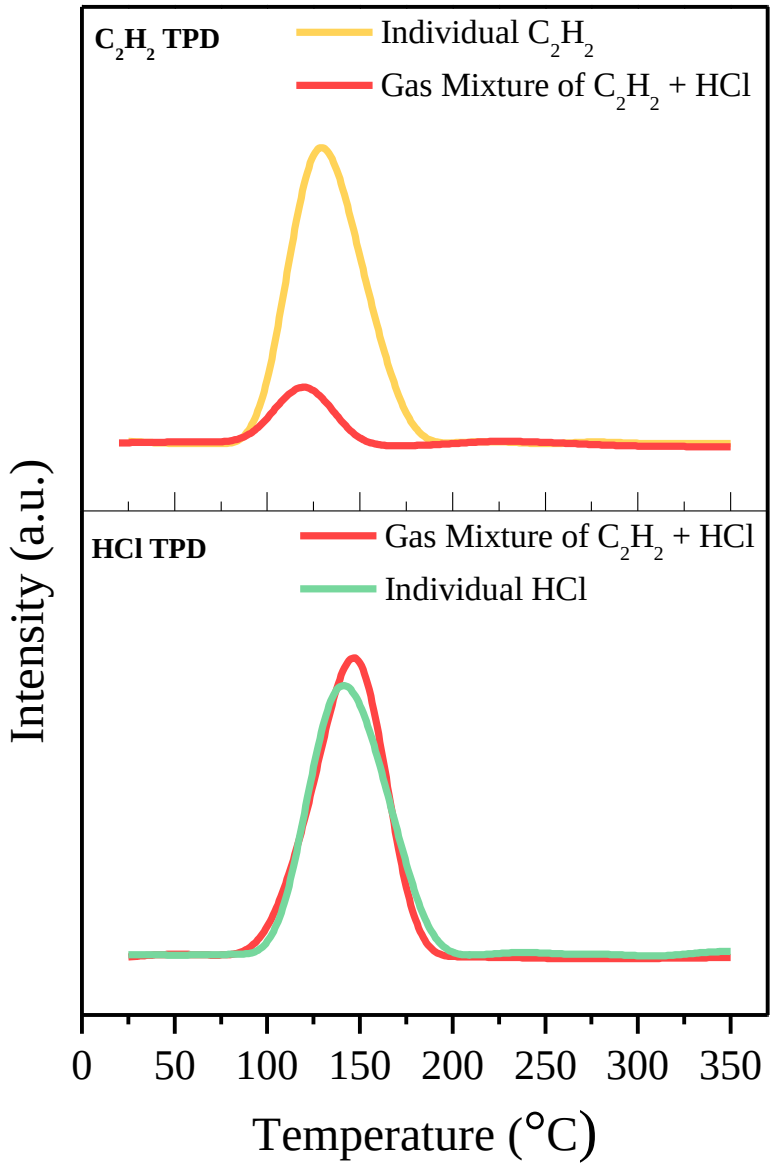

Figure S13 C_2H_2 and HCl TPD of RuO_2/C under individual gas (C_2H_2 or HCl) and gas mixture of [C_2H_2 + HCl].

The TPD results showed that large amount of HCl and C_2H_2 could be adsorbed on RuO_2/C when HCl and C_2H_2 were passed over the catalyst bed individually. However, when RuO_2/C was pretreated by the gas mixture of [C_2H_2 + HCl], C_2H_2 adsorbed contents was significantly reduced, suggesting competitive adsorption of HCl and C_2H_2 on Ru sites. HCl is preferentially adsorbed when the reactants flows through RuO_2/C catalyst.

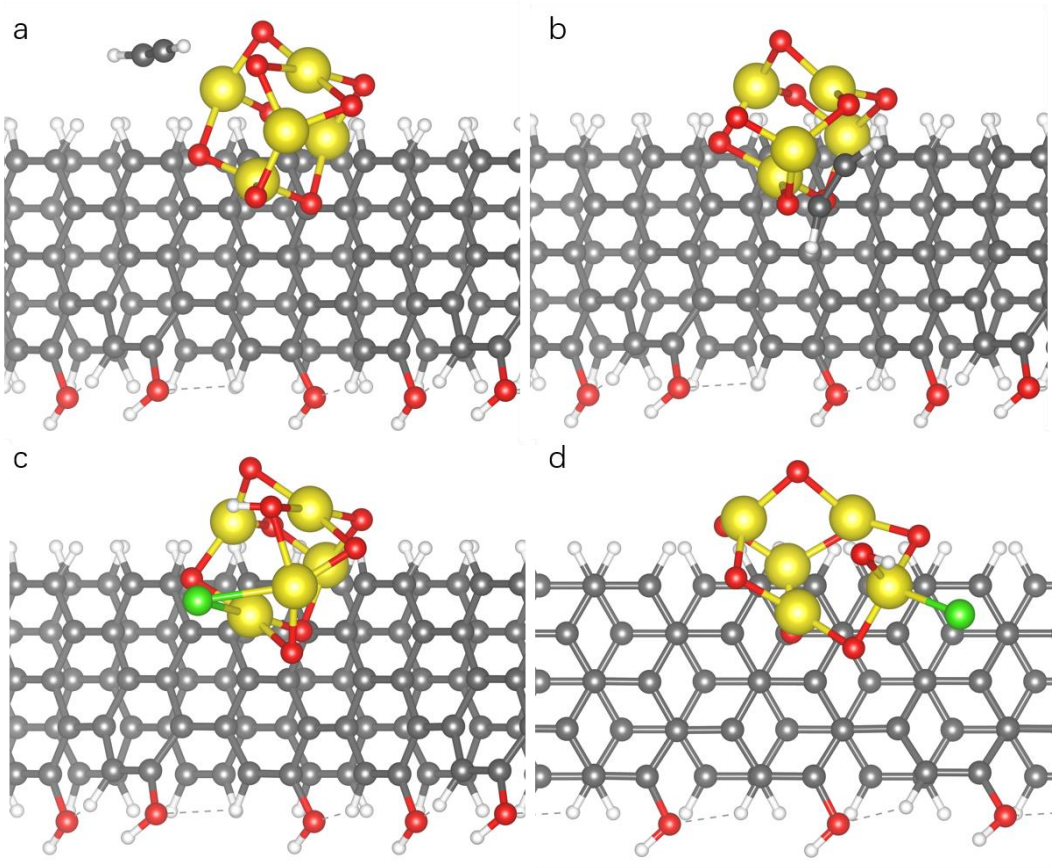

Figure S14 The adsorption C_2H_2 and HCl at sites on RuO_2/C sample. Adsorption sites 1 (a and c) and 2 (b and d) are different sites for C_2H_2 and HCl adsorbed on RuO_2/C. The red, gray (carrier), black (C_2H_2), green, white and yellow balls represent O, C (carrier and C_2H_2), Cl, H and Ru atoms, respectively.

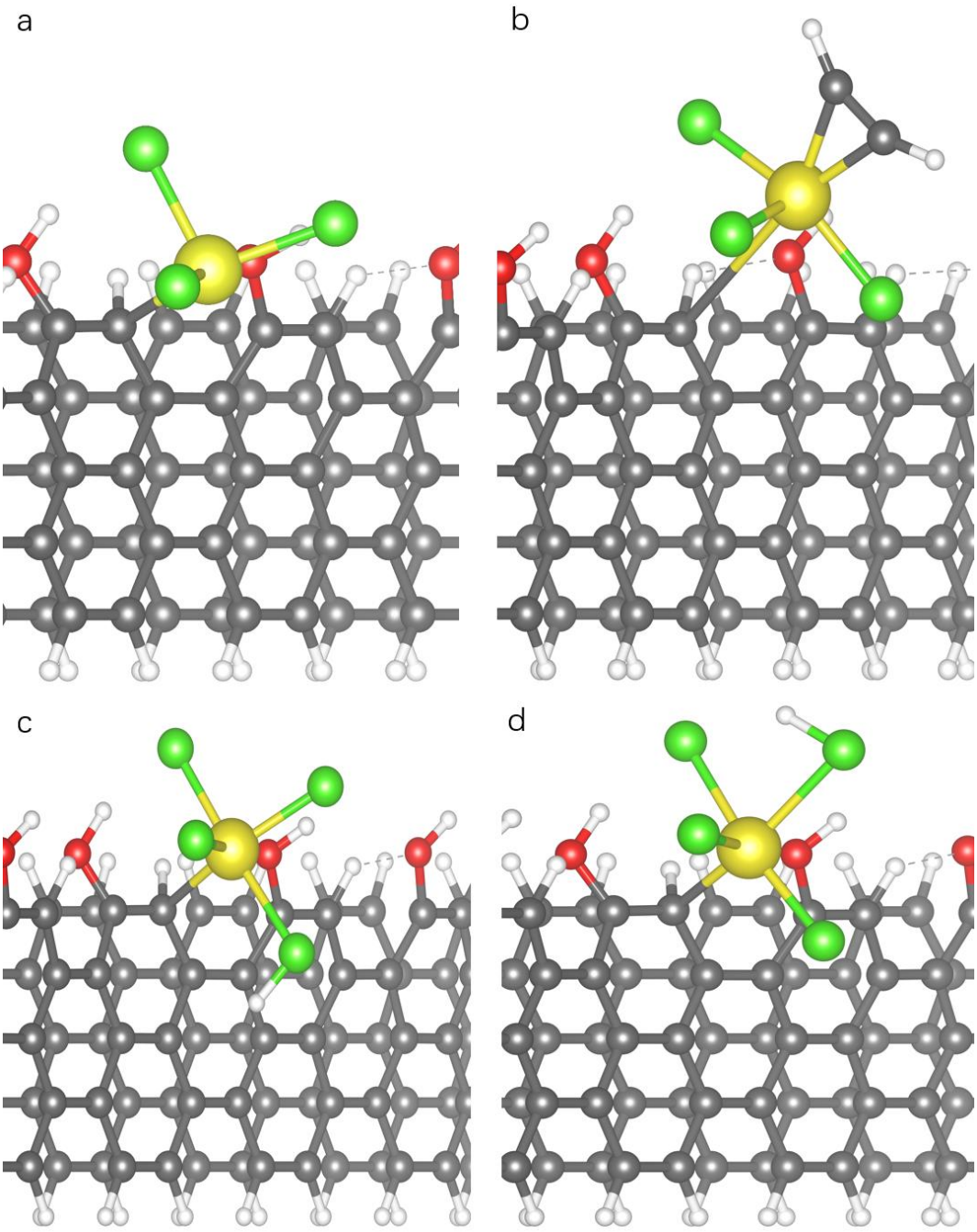

Figure S15 The adsorption C_2H_2 and HCl on Ru SAC sample at site 1 and site 2. Adsorption sites 1 (a and c) and 2 (b and d) are different sites for C_2H_2 adsorbed on $RuCl_3$ of Ru SAC. In this case, the adsorption energy is -101 $kJ \cdot mol^{-1}$. The red, gray (carrier), black (C_2H_2), green, white and yellow balls represent O, C (carrier and C_2H_2), Cl, H and Ru atoms, respectively.

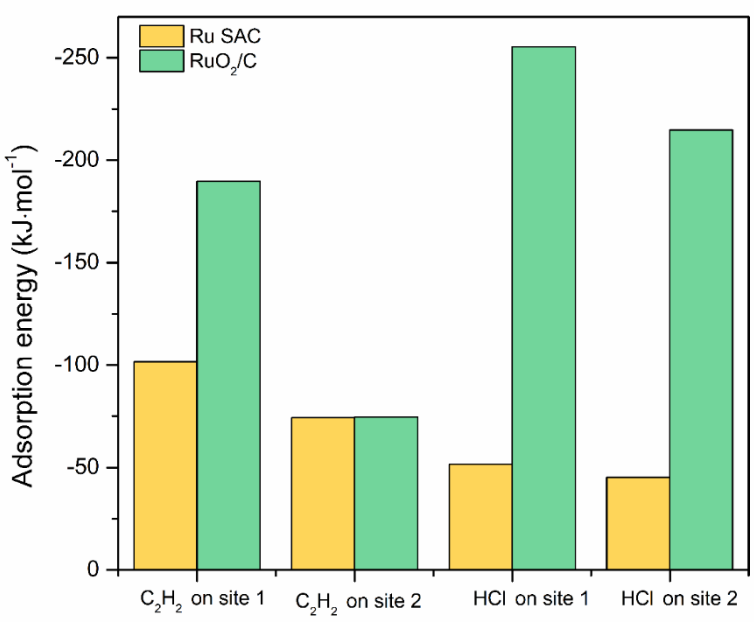

Figure S16 The adsorption energies of C_2H_2 and HCl on different Ru sites (Figure S14-S15).

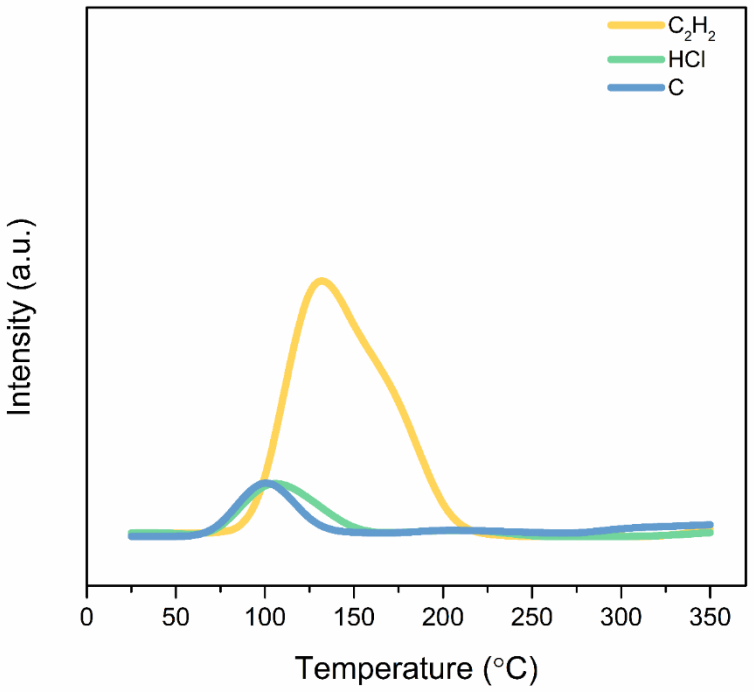

Figure S17 C_2H_2 and HCl TPD of Ru SAC under individual gas (C_2H_2 or HCl).

The adsorption amount of C_2H_2 on $RuCl_3$ in Ru SAC was higher than that of HCl (Figure 2b), and the HCl-TPD profiles for the catalysts and rare activated carbon carrier were very similar (Figure S17), suggesting the dominant adsorption properties of C_2H_2 on $RuCl_3$.

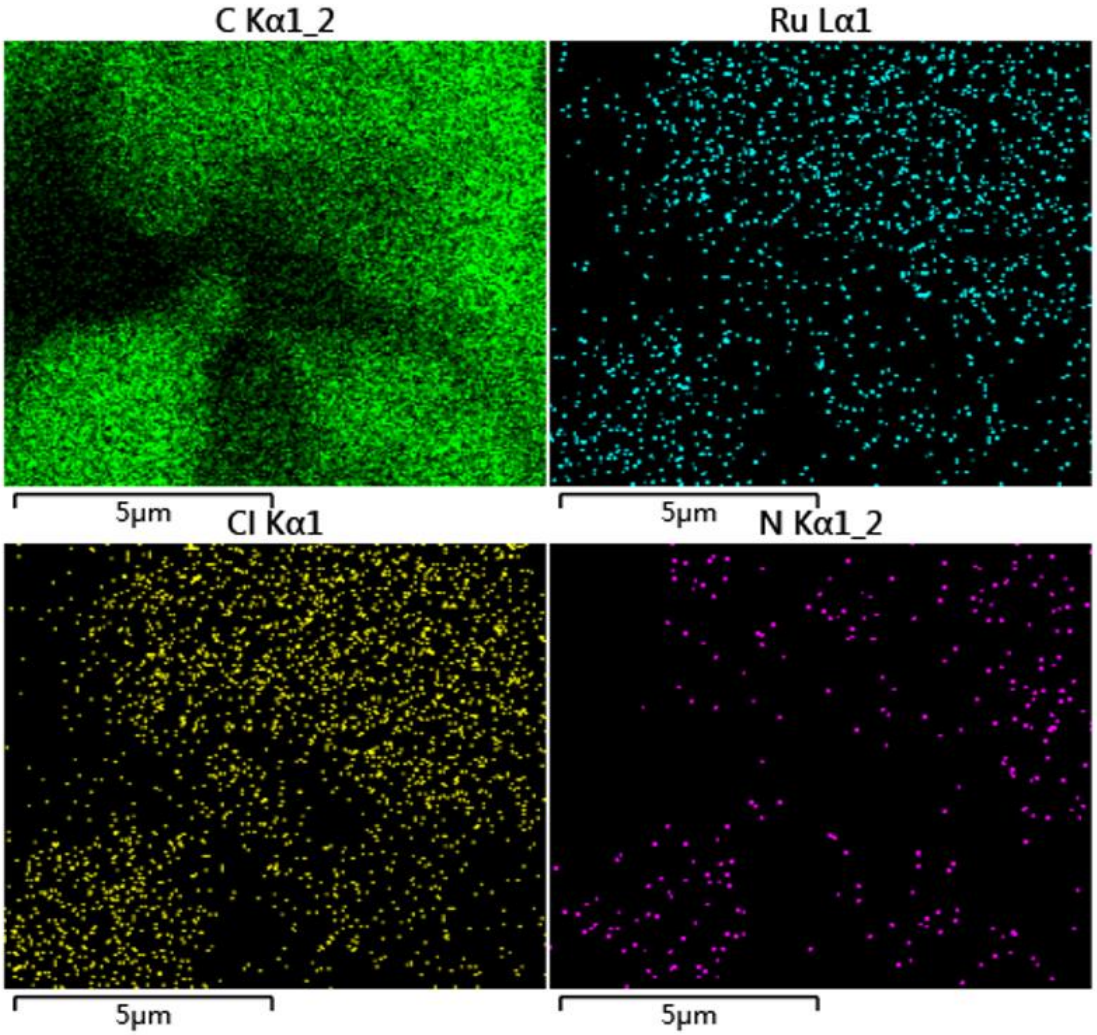

Figure S18 STEM images and elemental mapping of Ru-N SAC.

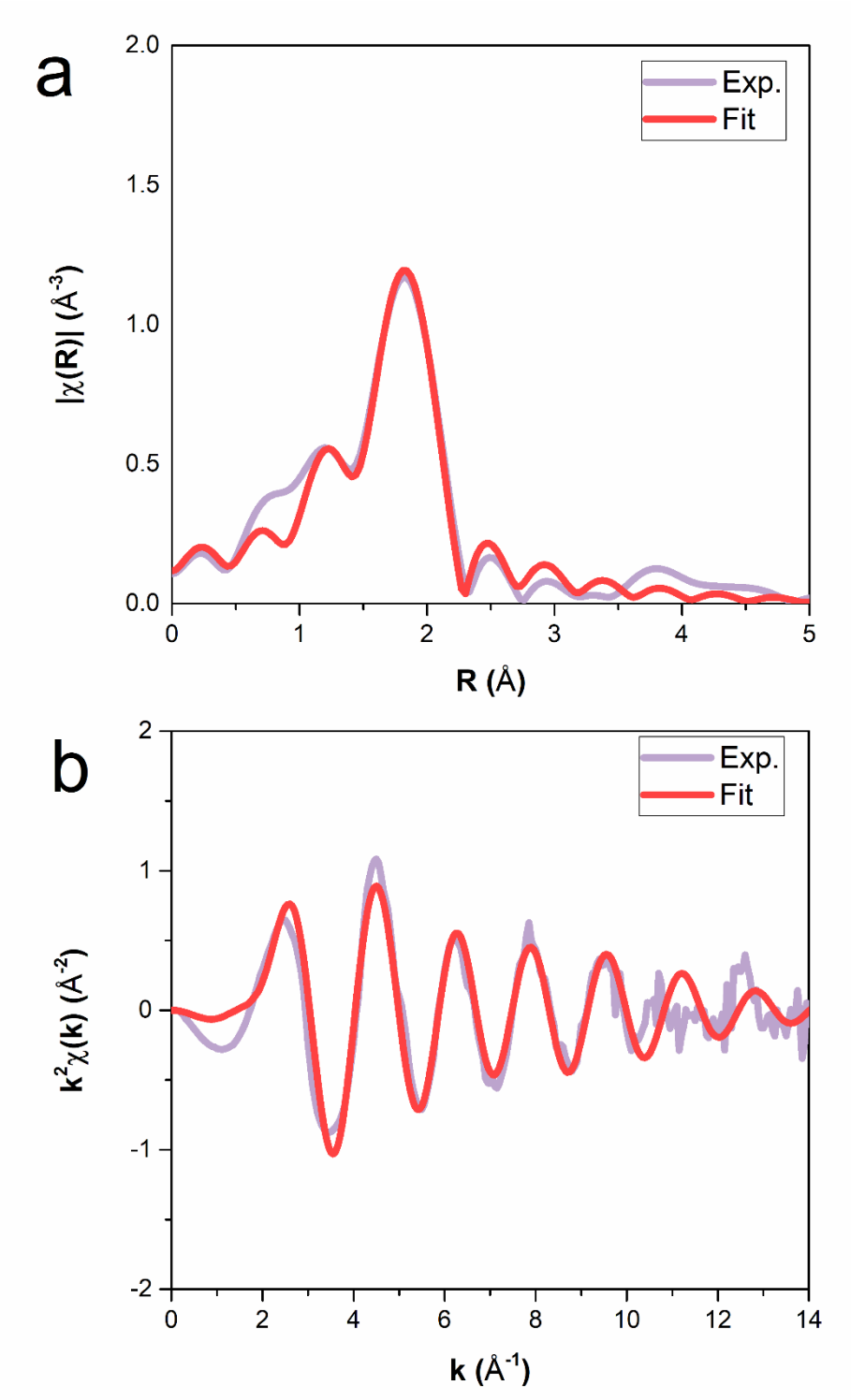

Figure S19 Ex situ Ru K edge-normalized XANES spectra of Ru-N SAC.

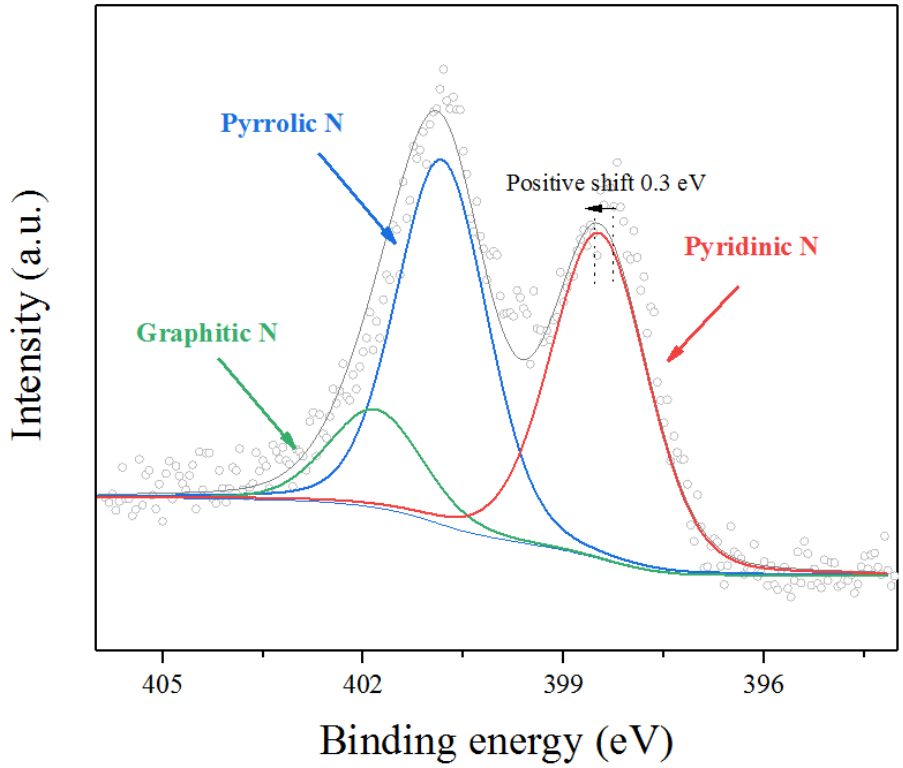

Figure S20 N1s XPS spectra of Ru-N SAC catalysts.

N1s XPS spectra showed that three possible types of N species were present (Figure S20): pyridinic N at around 398.6 eV, pyrrolic N at around 400.5 eV and graphitic N at around 401.3 eV [6-8]. We found that the binding energy of pyridinic-N species positively shifted from the standard 398.3 eV to 398.6 eV. Except for pyridinic-N, no similar phenomenon was found in the binding energy of pyridinic-N. In XPS analysis technology, ± 0.2 eV is considered as the system error range. Therefore, this result indicates that a strong interaction has occurred between the Ru atom and the pyridinic-N species.

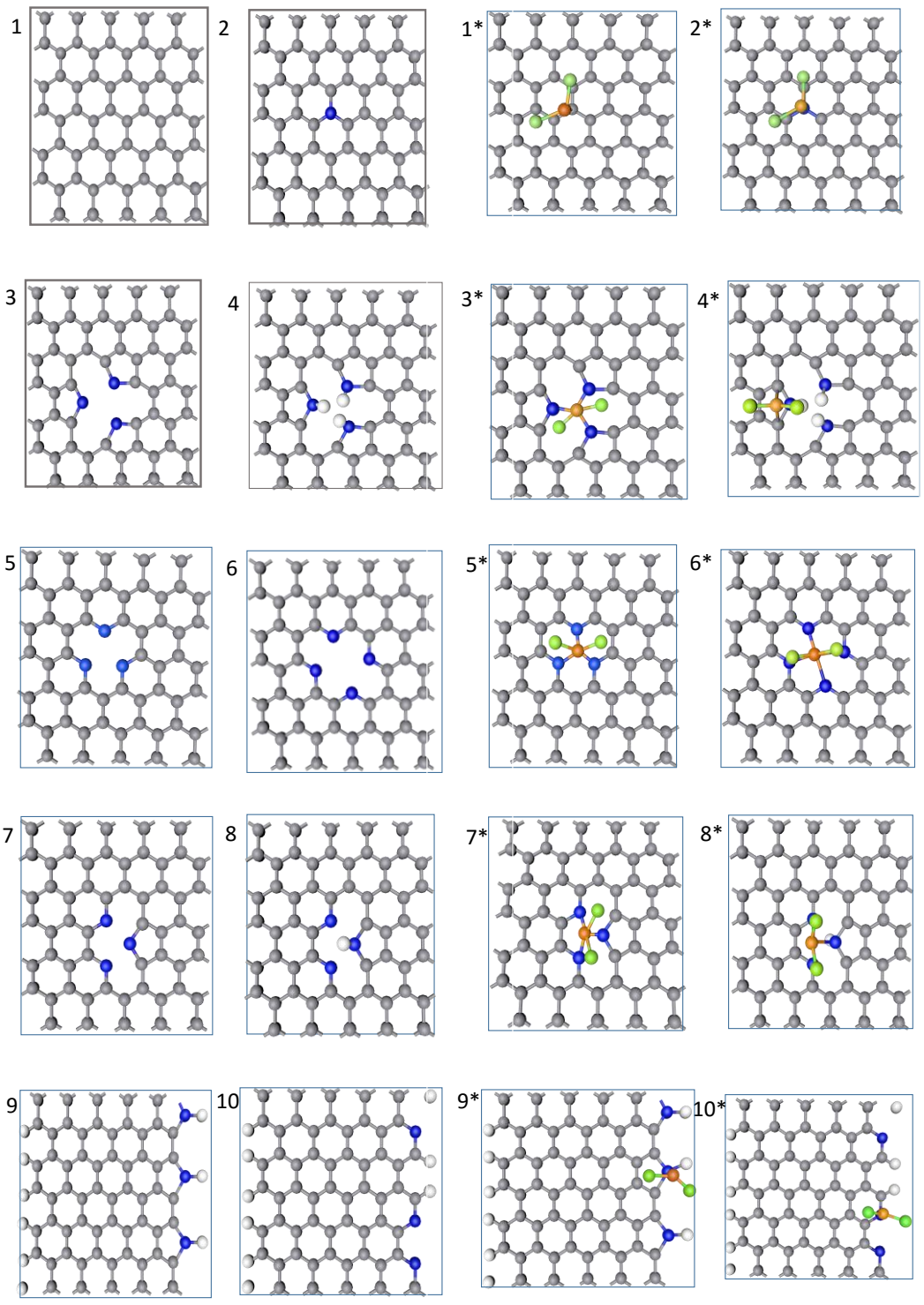

Figure S21 Schematic representation of the investigated Ru species adsorbed on distinct N sites. The gray, white, blue, light green and dark green balls represent C, H, N, Cl and Ru atoms, respectively.

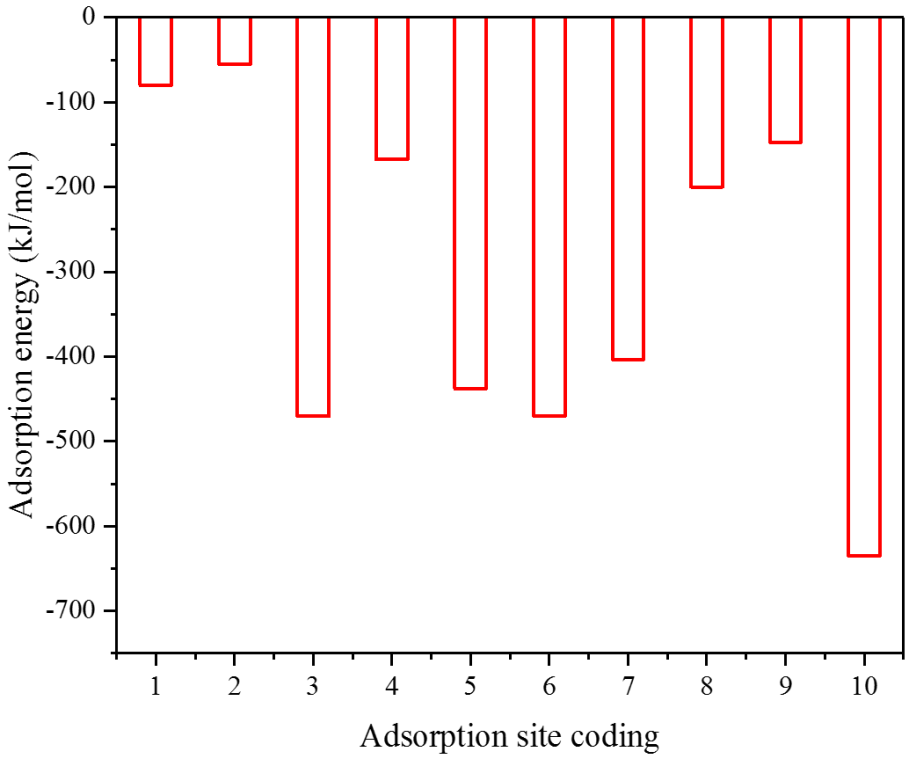

Figure S22 The adsorption energies of Ru species on distinct N sites.

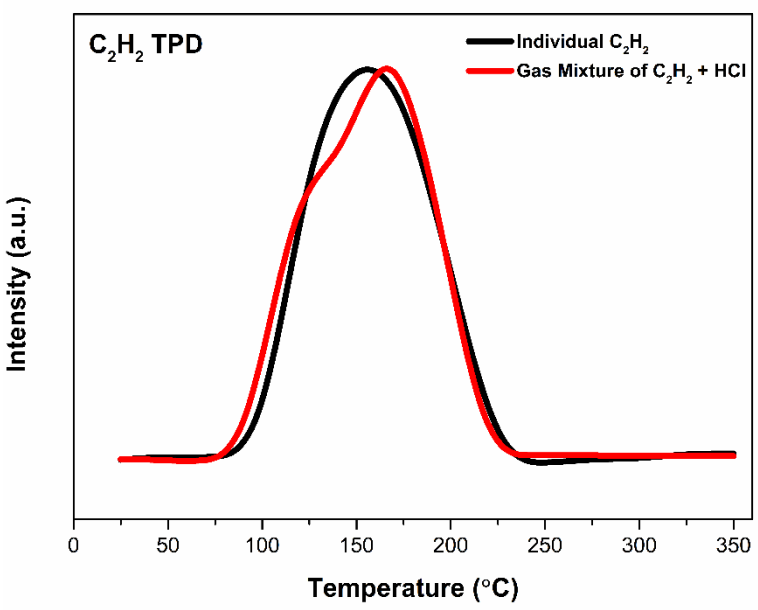

Figure S23 C_2H_2-TPD spectra of Ru-N SAC under individual gas (C_2H_2) and gas mixture [C_2H_2 + HCl].

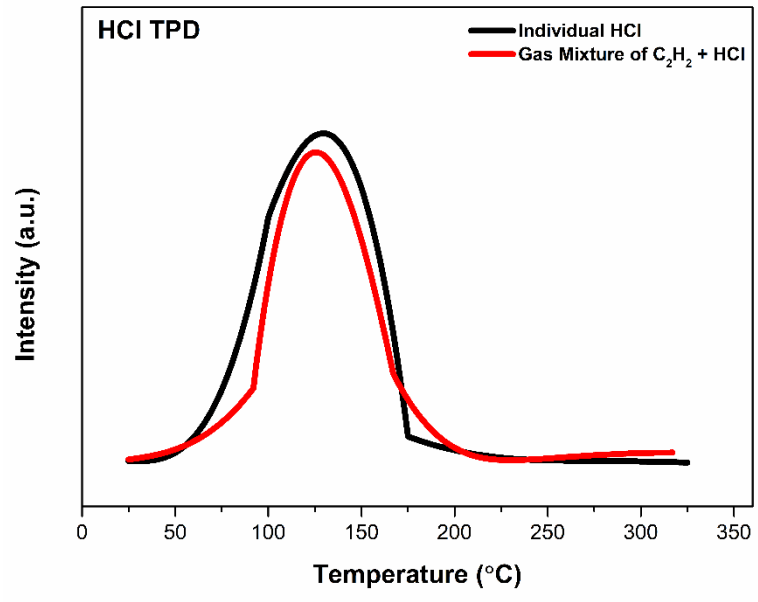

Figure S24 HCl-TPD spectra of Ru-N SAC under individual gas (HCl) and gas mixture [C_2H_2 + HCl

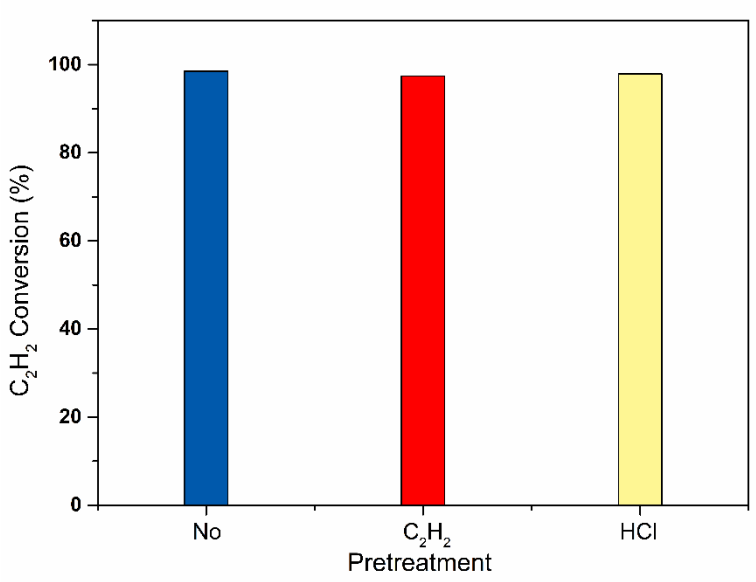

Figure S25 Pretreatment effects of C_2H_2 and HCl on the catalytic performance of Ru-N SAC in acetylene hydr ochlorination. The catalyst was pre-treated with the individual components at 160 °C for 2 h. Reaction conditions: 160 °C, C_2H_2 GHSV = 1000 h^{-1}, V(HCl)/V(C_2H_2) = 1.2.

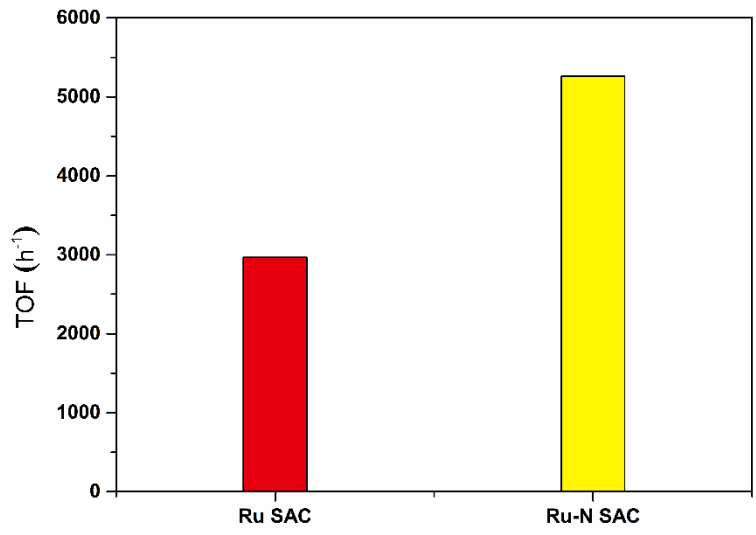

Figure S26 TOF values of Ru SAC and Ru-N SAC. Reaction conditions: 160 °C, C_2H_2 GHSV = 18000 h^{-1}, V(HCl)/V(C_2H_2) = 1.2.

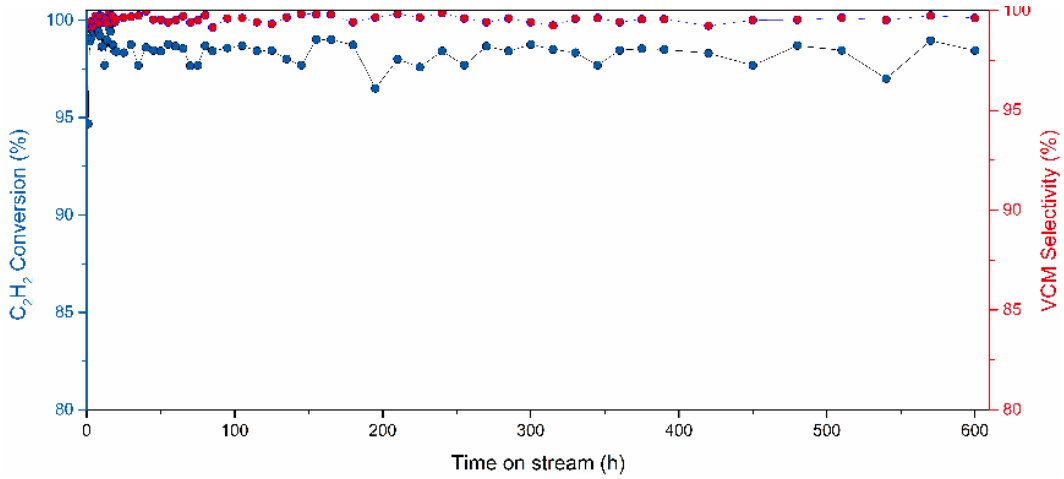

Figure S27 Long-term stability of Ru-N SAC catalyst. Reactions were carried out at 160 ℃, a space velocity GHSV (C_2H_2) of 50 h^{-1} , V(HCl)/V(C_2H_2) = 1.2, and reaction gas mixture with 250 ppm H_2S and 350 ppm H_2.

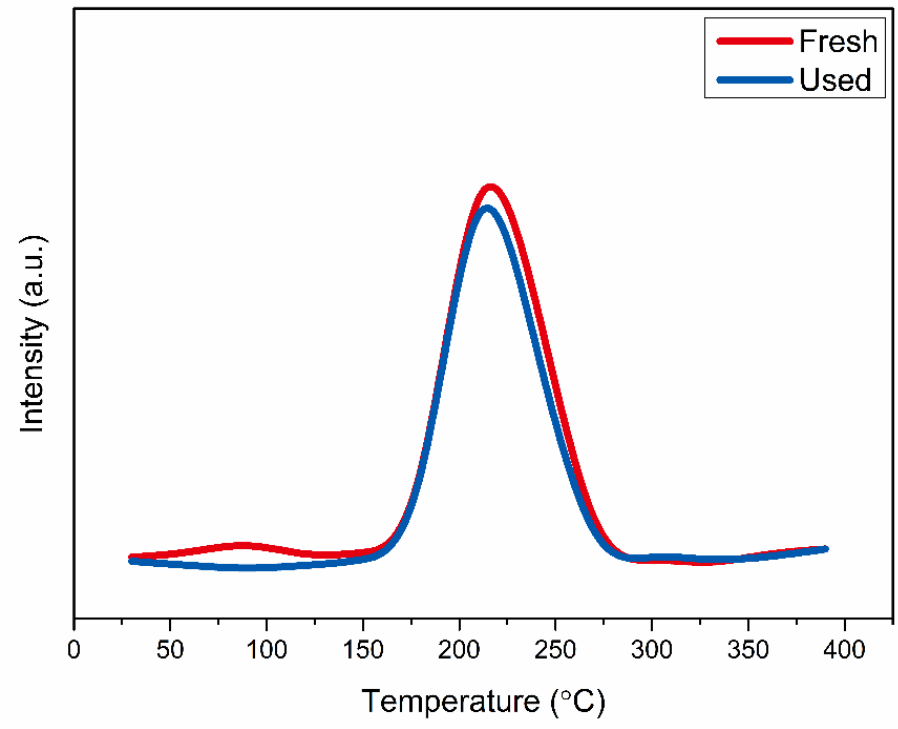

Figure S28 TPR profiles of fresh and Spent Ru-N SAC.

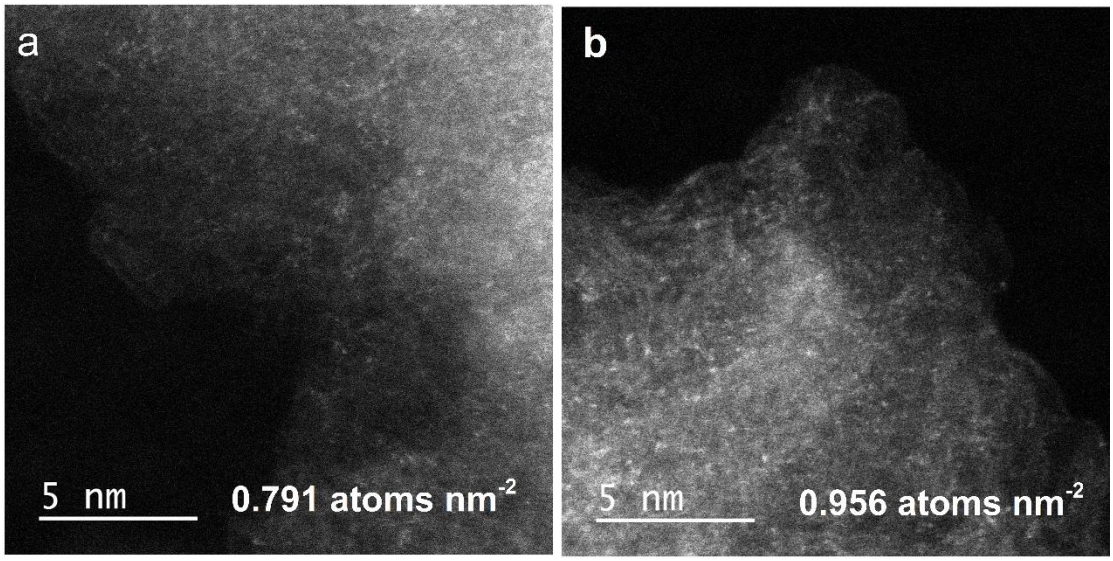

Figure S29 HAADF-STEM images for Ru-N SAC with 0.5 wt.% Ru mass loading. The atom density is expressed as the number of atoms in a unit region (atoms nm^{-2}). The average ruthenium atom density on the surface of the catalyst calculated from Figures a and b is 0.874 atoms nm^{-2}.

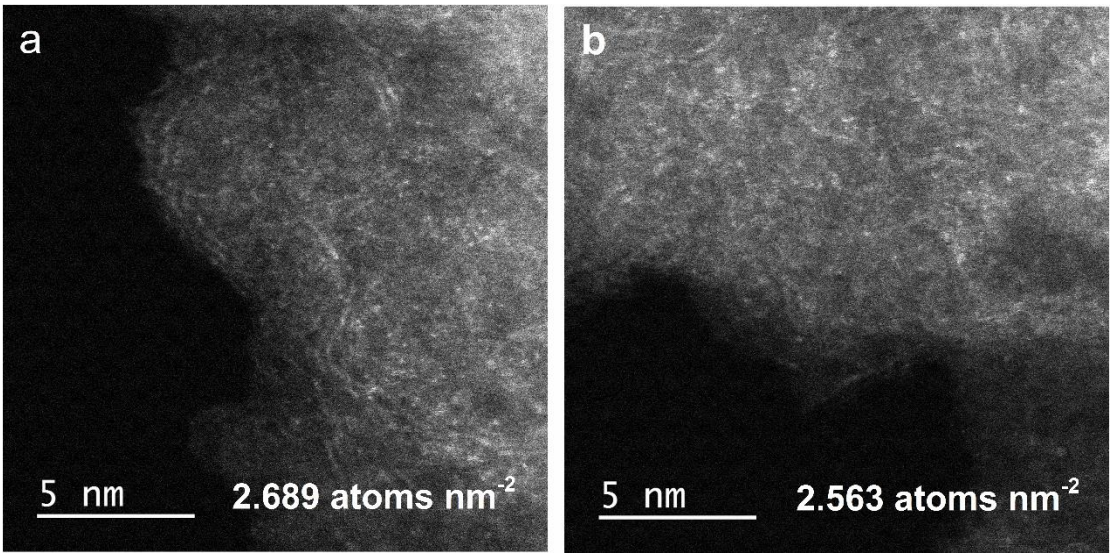

Figure S30 HAADF-STEM images for Ru-N SAC with 2.0 wt.% Ru mass loading. The atom density is expressed as the number of atoms in a unit region (atoms nm^{-2}). The average ruthenium atom density on the surface of the catalyst calculated from Figures a and b is 2.626 atoms nm^{-2}.

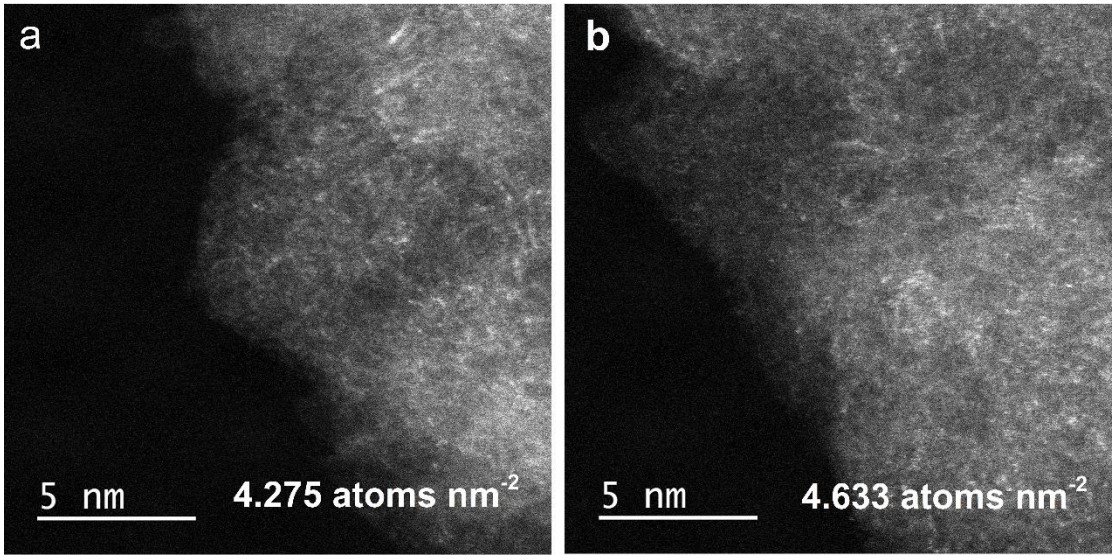

Figure S31 HAADF-STEM images for Ru-N SAC with 4.0 wt.% Ru mass loading. The atom density is expressed as the number of atoms in a unit region (atoms nm^{-2}). The average ruthenium atom density on the surface of the catalyst calculated from Figures a and b is 4.454 atoms nm^{-2}.

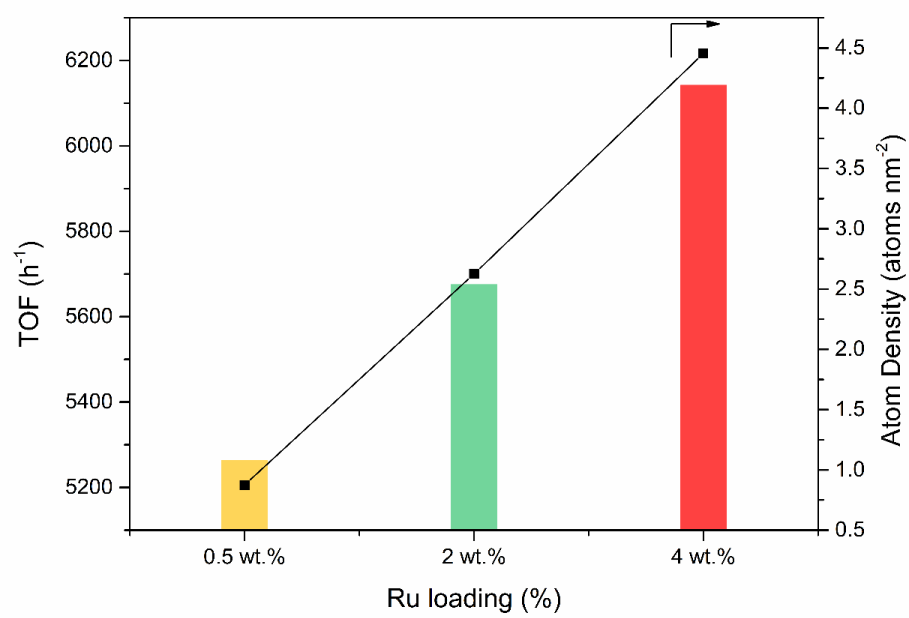

Figure S32 TOF of Ru-N SAC with different Ru mass loading. Reaction conditions: 160 °C, C_2H_2 GHSV = 18000 h^{-1}, V(HCl)/V(C_2H_2) = 1.2.

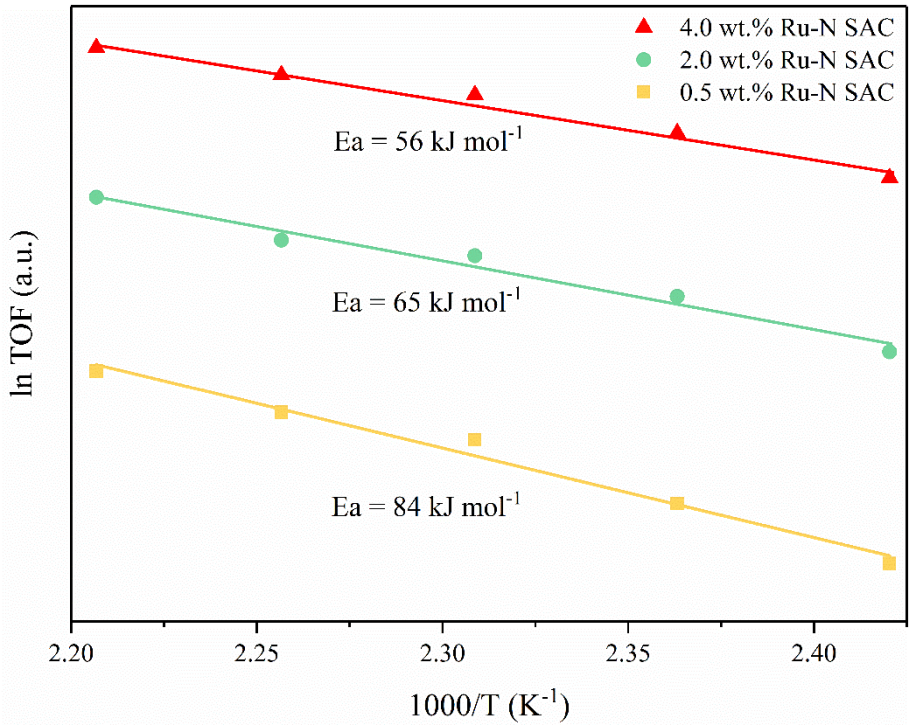

Figure S33 The apparent activation energy (Ea) of Ru-N SAC with different Ru mass loading. Reaction conditions: C_2H_2 GHSV = 18000 h^{-1}, V(HCl)/V(C_2H_2) = 1.2. In order to circumvent the influence of catalyst deactivation, each point was obtained in a single experiment.

References

[1] J. Zhao, S. Gu, X. Xu, T. Zhang, Y. Yu, X. Di, J. Ni, Z. Pan, X. Li, *Catal. Sci. Technol*. 2016, 6, 3263-3270.

[2] Y. Pu, J. Zhang, L. Yu, Y. Jin, W.i Li, *Appl. Catal. A: Gen.* 2014, *488*, 28-36.

[3] H. Li, B. Wu, F. Wang, X. Zhang, *ChemCatChem* 2018, *10*, 4090-4099.

[4] H. Zhang, W. Li, Y. Jin, W. Sheng, M. Hu, X. Wang, J. Zhang, *Appl. Catal. B: Environ*. 2016, 189, 56-64.

[5] X. Xu, H. He, J. Zhao, B. Wang, S. Gu, X. Li, *Chin. J. Chem. Eng*. 2017, 25, 1217-1221.

[6] J. Zhao, B. Wang, Y. Yue, G. Sheng, H. Lai, S. Wang, L. Yu, Q. Zhang, F. Feng, Z.-T. Hu, X. Li, *J. Catal.* 2019, *373*, 240-249.

[7] B. Wang, J. Zhao, Y. Yue, G. Sheng, H. Lai, J. Rui, H. He, Z.-T. Hu, Q. Zhang, L. Guo, X. Li, *ChemCatChem* 2019, *11*, 1002-1009.

[8] X. Li, X. Pan, L. Yu, P. Ren, X. Wu, L. Sun, F. Jiao, X. Bao, *Nat. Commun.* 2014, *5*.

[9] S. K. Kaiser, R. Lin, S. Mitchell, E. Fako, F. Krumeich, R. Hauert, O. V. Safonova, V. A. Kondratenko, E. V. Kondratenko, S. M. Collins, P. A. Midgley, N. Lopez, J. Perez-Ramirez, *Chem. Sci.* 2019, *10*, 359-369.

[10] a) D. E. Mears, *J. Catal.* 1971*, 20,* 127-131; b) Weisz, P. B., Prater, C. D, *Adv. Catal*. 1954, 6, 143-196; c) H.S. Fogler, Elements of Chemical Reaction Engineering, *Prentice Hall Professional Technical Reference*, 2006; d) R. Perry, D. Green, Perry's Chemical Engineers' Handbook, Eighth Edition, *McGraw-Hill Education*, 2008.